Microporous and Mesoporous Materials 141 (2011) 128–134

Contents lists available at ScienceDirect

Microporous and Mesoporous Materials

journal homepage: www.elsevier.com/locate/micromeso

Mesoscale porous silica as drug delivery vehicles: Synthesis, characterization, and pH-sensitive release profiles

Peter DeMuth [a], Matthew Hurley [a], Chunwei Wu [b], Stephanie Galanie [a], Michael R. Zachariah [a,b], Philip DeShong [a,*]

[a] Department of Chemistry and Biochemistry, University of Maryland, College Park, MD 20742, USA
[b] Department of Mechanical Engineering, University of Maryland, College Park, MD 20742, USA

ARTICLE INFO

Article history:
Received 24 August 2010
Received in revised form 21 October 2010
Accepted 21 October 2010
Available online 30 October 2010

Keywords:
Mesoporous silica nanoparticles
Controlled release
pH responsive

ABSTRACT

Mesoporous silica nanoparticles (MSN) have potential as drug delivery and controlled release devices due to their high surface area and absorption capabilities. The effect of surface charge and pH on the release of the fluorescent dye, rhodamine 6G, from MSN has been studied. Release profiles of rhodamine 6G from bare and amine-coated MSN at pH 5.0 and 7.4 are very different and demonstrate that electrostatic interactions between entrapped rhodamine 6G molecules and the charged surface of the MSN have a significant effect on release kinetics. Release of rhodamine 6G from amine-coated MSN can be fit to a single exponential function, while release from bare MSN can be fit to a double exponential function—indicating that the release of rhodamine 6G from bare MSN is a two-phase process. In addition, it was determined that MSN need to be sonicated in dye solution to maximize their loading capacity.

1. Introduction

Since the Mobil Corporation first introduced Mobil Crystalline Material (MCM)-41 [1], a large body of research has been devoted to developing novel mesoporous silica materials with controlled pore size and uniform pore structure, such as Santa Barbara amorphous silica (SBA)-15 [2], Michigan State University silica (MSU)-n [3], folded sheet-derived mesoporous silica (FSM)-16 [4], and Korean Institute of Technology silica (KIT)-1 [5–7]. These materials were originally used as catalysts and absorption/purification materials [1,7]. More recently, mesoporous silica nanoparticles (MSN) have gained attention for their potential as controlled release systems and vehicles for the delivery of chemotherapeutics due to their high surface areas, large cavity volumes, and ability to be functionalized with biomolecules for the targeting of specific tissue populations [6–38]. Despite their promise, silica and alumina mesoporous nanospheres have not been utilized extensively for drug delivery because imposing hurdles remain before they can be used in clinical settings, including control of particle dispersity, control of pore size and density, and control of release dynamics.

Vallet-Regi and coworkers were the first to study MCM-41 material as drug delivery systems and proved that MCM-41 could be used to absorb and then later release ibuprofen [8]. Since their initial work, they and others have demonstrated that surface-functionalization [9–13,24], pore size [14–16], pore structure [15–17], loading conditions [18], as well as the chemical characteristics of the loaded analyte [18,19] affect both the absorption and release of the analyte into and out of porous silica material. Importantly, these studies show that attractive [9] and repulsive [13] electrostatic interactions as well as hydrophobic effects [24] between the entrapped molecules and the silica surface affect the rate of release from these porous materials. Recently, Ng et al. used confocal laser scanning microscopy to show that cationic molecules have a different release profile than anionic molecules from mesoporous silica spheres due to the affinity between the cationic molecules and the negatively charged silica surface [19].

While the above systems utilize pore size and electrostatic interactions for controlled release, others have developed more complex systems in which stimuli responsive capping agents, supramolecular assemblies, or polymers are employed to control the release of guest molecules. Fujiwara demonstrated the potential of stimuli responsive controlled release devices by controlling the uptake and release of guest molecules into and out of coumarin-functionalized MCM-41 using UV radiation [26]. Lin and coworkers have designed several systems in which CdS or gold nanoparticles are used to "cap" loaded MSN. The nanoparticles can be removed from the surface of the MSN upon the addition of a reducing agent or by irradiating the system with 365 nm light [6,7,20–22]. Zink and Stoddart have made controlled release systems from mesoporous silica films and particles using supramolecular nanovalves that are governed by redox chemistry [27–29], pH [30–33], or light [34]. Kim has also reported a gated-release system

* Corresponding author.
E-mail address: deshong@umd.edu (P. DeShong).

1387-1811/$ - see front matter © 2010 Elsevier Inc. All rights reserved.
doi:10.1016/j.micromeso.2010.10.035

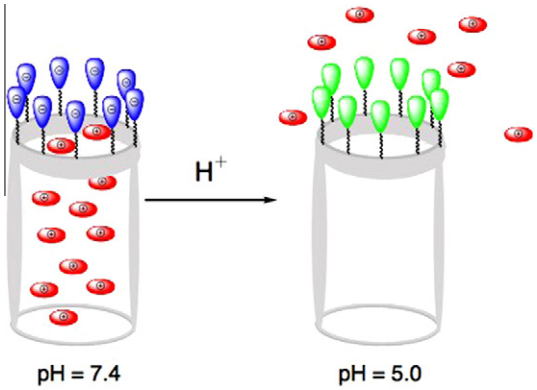

Fig. 1. Schematic representation of a pH driven controlled release device.

utilizing a pH responsive supramolecular motif on the MSN surface [35]. Additionally, You and coworkers have reported temperature-controlled release devices utilizing a surface bound temperature-responsive polymer [25], while Hong has created a system in which release is governed by a pH responsive polymer [36]. Lin et al. have also designed insulin loaded MSN that are sealed with glucose responsive proteins [23]. And, very recently, Wang coated the surface of MSN with polyelectrolyte multilayers to obtain a controlled release system that is responsive toward reducing agents [37].

It has been demonstrated that aerosol sol–gel synthesis techniques can be applied to the preparation of novel silica-based nanoparticles and have significant advantages of solution phase methodologies [39–41]. These advantages include: (1) the ability to control pore diameter and density by including either inorganic salts or surfactants in the sol–gel aerosol solution, and (2) the ability to prepare particles with highly uniform dispersity employing electrostatic separation on the resulting particle mixture. Accordingly, this technique should be applicable to drug delivery vehicles and would overcome many of the limitations of MSN prepared by the solution methods described above.

It is established that MSN can be taken into a cell through endocytosis [7,42]. The pH inside an endosome is lower than cytosolic environment in a cell [43]. Thus, one can anticipate that a release strategy that employs pH as a trigger for release would be particularly attractive [32]. Ultimately, our goal is to create a MSN drug delivery system that shows no release at normal physiological pH (7.4) and fast release at pH 5, the typical pH within an endosome (Fig. 1). This type of delivery system would ensure that the entrapped drug would be released from the nanoparticle only after the nanoparticle has been endocytosed into the target tissue. Herein, we report on our initial steps toward such a system and the work that has been done to better understand how surface coverage and pH affect the release of the cationic dye, rhodamine 6G, from mesoporous silica nanoparticles created in our lab via aerosol sol–gel synthesis methodology.

2. Experimental

2.1. General

All materials were used as received from the supplier. Rhodamine 6G (R6G) was obtained from Sigma Aldrich (BioChemika, for fluorescence: 83697). (3-Aminopropyl)triethoxysilane (APTES) was obtained from Sigma Aldrich (Fluka: 09324). Tetraethyl orthosilicate was obtained from Sigma Aldrich. Pluronic® F-127 was obtain from BASF. All aqueous solutions were made using water filtered through a Millipore water filtration system unless otherwise indicated. Phosphate buffered saline (PBS) solutions were prepared from phosphate buffered saline tablets obtained from Sigma Aldrich (Sigma, tablets: P4417) as directed. The PBS solutions prepared had a measured pH of 7.4. Acetic acid (0.78 mL, 13.63 mmol) and sodium acetate (2.88 g, 35.11 mmol) used to prepare the acetate buffer (400 mL, pH 5.0) were obtained from J.T. Baker. An Ocean Optics USB 2000 Spectrometer was used to measure the absorbance (A) of the supernatant during release studies. A Bransonic 321 desk sonicator was used to sonicate MSN samples. Zeta potentials were measured using a Zetasizer Nano ZS90 from Malvern Instruments Ltd. BET and BJH measurements were obtained using a Micromeritics Tristar II 3020 Surface Area Analyzer. The surface area of standard silica–alumina pellets received from Micromeritics was measured to verify the instrument was in proper working condition.

2.2. Fabrication of MSN

MSN were fabricated by a template-assisted sol–gel process that was implemented via aerosol technique. Aerosol droplets were created from a stainless steel pressure atomizer containing the precursor mixing solution consisting of tetraethyl orthosilicate (2.6 g, 13 mmol) and Pluronic® F-127 (0.55 g, 0.04 mmol) dissolved in absolute ethanol (17.3 mL) and deionized water (9.0 mL) adjusted to pH 1.2 with HCl. Droplets being carried through a stainless steal tube by dried air passed through a diffusion-dryer to remove most of the solvent and then through a tube furnace at 400 °C. Normal residence time was 1 s under the gas flow rate of 3.5 L/min used in the experiments. Particles were collected on a 0.2 μm pore Millipore HTTP membrane filter housed in a stainless steel holder (covered by heating tape to prevent re-condensation of solvent vapor). After being removed from the membrane, particles were calcined at 500 °C for 4 h to remove the surfactant, yielding MSN.

2.3. Gravity filtration

A 2.0 mg/mL stock suspension of MSN (100 mg) in Millipore water (50 mL) was made, vortexed, and then sonicated using a Bransonic 321 desk sonicator for 30 min. The suspension was then allowed to settle for 24 h. The upper 45 mL of supernatant was removed by pipette and the remaining retentate was diluted back to 50 mL using fresh Millipore water. The suspension was vortexed and then sonicated for 30 min. This procedure was repeated three times. The particles remaining after the fourth cycle were dried in vacuo and were used in the release studies.

2.4. Rhodamine 6G loading

The MSN comprising the retentate (dried) remaining after the gravity filtration process were added to a 0.15 mg/mL solution of rhodamine 6G in PBS buffer to make a 2 mg/mL suspension of MSN in rhodamine 6G solution. The suspension was vortexed and then sat undisturbed for 48 h. The particles were sonicated in the 0.15 mg/mL rhodamine 6G solution where indicated.

2.5. MSN functionalization

An aliquot of the MSN/rhodamine 6G suspension was removed from the stock solution and sonicated for 30 min. (3-Aminopropyl)triethoxysilane (APTES) was added to the aliquot to yield a 0.1 mL APTES/mg MSN solution. The reaction mixture stirred at room temperature for 10 min and was then centrifuged. The supernatant was removed. The functionalized MSN were immediately used in a release experiment.

2.6. Rhodamine 6G release quantification using UV–Vis spectroscopy

An aliquot of the MSN/rhodamine 6G suspension (5.0 mL) was removed from the stock solution and sonicated for 30 min. The sample suspension was then centrifuged and the supernatant was removed by pipette. The particles were washed with PBS buffer (5.0 mL) and centrifuged for 5 min. The supernatant was removed via pipette. The washing process was repeated twice more. After the final washing process, the MSN were resuspended in buffer solution at the desired pH and 25 °C. PBS buffer was used for release at pH 7.4, while acetate buffer was used for release at pH 5.0. A 2.0 mL aliquot was removed from the suspension and centrifuged. The absorbance of the supernatant was measured using an Ocean Optics USB 2000 Spectrometer. The analyzed supernatant and the 2.0 mL aliquot were then returned to the sample suspension. This process was repeated every twenty minutes until no further release was observed.

2.7. Mathematical modeling of release from MSN

For each release profile, GraphPad Prism was used to perform nonlinear least squares fitting to both a double exponential and a single exponential function, and the best fit model was chosen using the extra sum-of-squares F test.

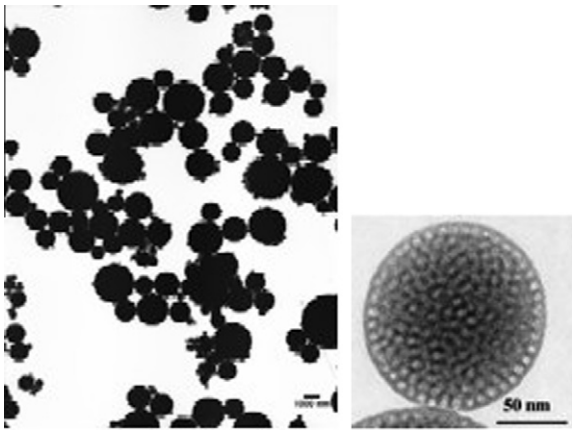

Fig. 2. TEM image of MSN used in release studies. The figure on the right shows the porous character of the particles.

The double exponential function, which describes two processes that have rates proportional to the diffusivity and the local concentration of the dye is defined as

$$M = S_1(1 - e^{-k_1 t}) + S_2(1 - e^{-k_2 t}) \quad (1)$$

where S_1 is the amount released during the first phase, S_2 is the amount released during the second phase, k_1 is the rate constant of the first phase, k_2 is the rate constant of the second phase, and S_1 and S_2 are related by

$$S_1 = P(100 - F_2)(0.01) \quad (2a)$$

$$S_2 = P(F_2)(0.01) \quad (2b)$$

where P is the total amount released and F_2 is the percent of release that occurs in the second phase.

The single-phase exponential function is defined as

$$M = P(1 - e^{-kt}) \quad (3)$$

where P is the total amount released and k is the rate constant.

3. Results and discussion

3.1. Characterization of MSN

To ensure the presence of colloidal material would not interfere with measuring the UV–Vis absorbance of the supernatant during the kinetic release studies, a gravity filtration technique (described above) was employed to obtain MSN of appropriate size. The larger particles comprising the retentate after the final filtration cycle were used in the kinetic release studies because they can be quickly and easily separated from the supernatant via centrifugation. Dynamic light scattering showed that the MSN used in the kinetic release studies had an average diameter of 1.6 μm. Though the particles are micron-sized, we propose that they are an appropriate model for nano-scale systems since the pore size and pore diameter of all particles are identical. Fig. 2 depicts TEM images of the MSN.

To quantify the porous nature of the particles, BET gas sorptometry was conducted. The surface area of the particles was measured to be 206.88 m^2/g. Though the BET surface area of our MSN is less than other MSN materials [1–3,8,20], the adsorption/desorption isotherms (Fig. 3) are indicative of typical mesoporous systems, having type IV physisorption isotherms with H2 hysteresis. The H2 hysteresis and the forced closure of the hysteresis loop indicate random pore distribution and an interconnected pore system [44].

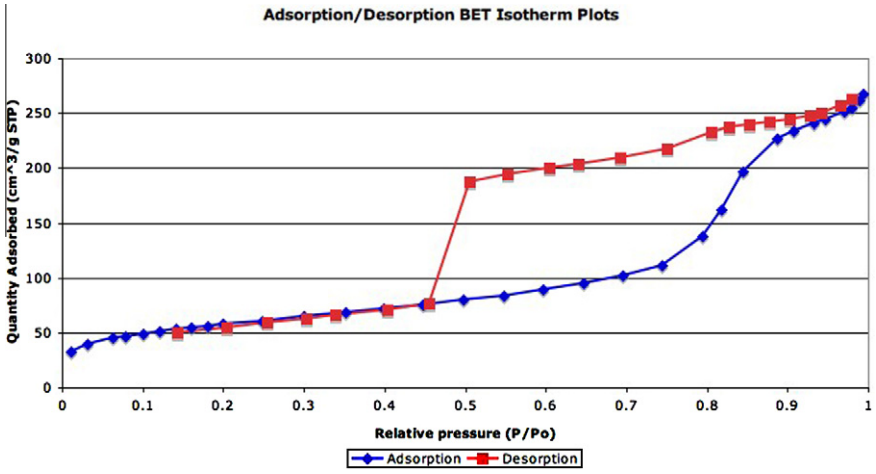

Fig. 3. Adsorption/desorption BET isotherms.

Table 1
Zeta potential measurements of APTES-coated and bare MSN at pH 7.4 and 5.0.

MSN type	pH	Zeta potential (STD) (mV)
Bare	7.4	−25.5 (1.2)
Bare	5.0	−3.40 (0.54)
APTES-coated	7.4	+12.2 (2.2)
APTES-coated	5.0	+41.1 (1.0)

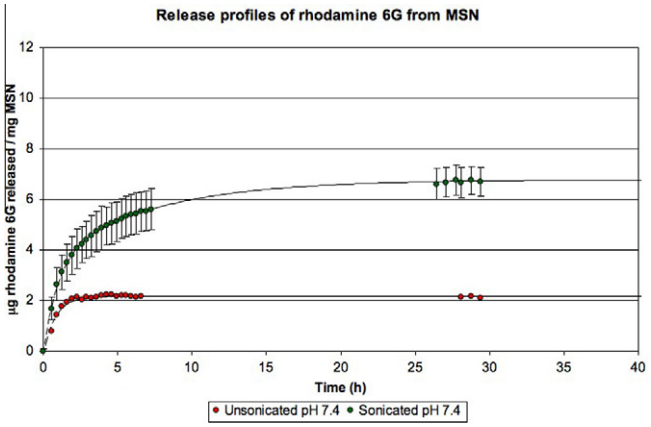

Fig. 4. Release of R6G from MSN with and without sonication.

The cumulative volume of the pores was calculated to be 0.42 cm^3/g, and the average pore width was calculated as 86.12 Å. The cumulative pore volume and average pore width were calculated using the BJH model from the adsorption isotherm branch.

The zeta potentials of both non-coated (bare) and APTES-coated MSN were measured at pH 7.4 and 5.0 in buffer solution having an ionic strength (I) of 0.16 M to quantify the surface charge of the particles under the release conditions. The zeta potential measurement results are shown in Table 1. As expected, the amine-functionalized MSN have positive potentials, while the bare MSN have negative potentials. In addition, the APTES-coated particles have a greater positive potential, and the bare MSN have a smaller negative potential at pH 5.0 than at 7.4, which was anticipated due to the increased acidity of the solution. It should be noted that the zeta potential measurements for the bare MSN at pH 5.0 were not reproducible (12 trials were required to obtain three measurements that were of good quality) which can be attributed to the fact that the particles were near their point of zero-charge.

3.2. Loading and release studies

There are several features of MSN that need to be evaluated if these materials are to serve as drug delivery systems: (1) loading efficiency, (2) pH-dependent release kinetics, and (3) the effect of surface modification on pH-dependent release kinetics.

In the course of our studies, we discovered that the MSN must be sonicated in dye solution to maximize loading. Fig. 4 shows the difference in release profiles of rhodamine 6G (R6G) from MSN that were sonicated in dye solution versus MSN that were only allowed to soak in dye solution and were not sonicated. All loading conditions were identical except for sonication, and the release experiments were conducted in PBS buffer at 25 °C. Though our goal was to mimic release under physiological conditions (i.e. 37 °C), all release experiments were performed at 25 °C because the release of rhodamine 6G at 37 °C is too rapid for kinetic data to be obtained using our methodology. The results clearly indicate that sonication increases the amount of dye that is loaded into the MSN; simply letting the particles soak in dye solution does not optimize their loading capacity. MSN that were sonicated in dye solution released ~4.5 µg of R6G/mg of MSN more than MSN that were not sonicated.

Analysis of the release profiles from sonicated and unsonicated MSN revealed an interesting phenomenon. The release of R6G from unsonicated bare MSN at pH 7.4 was best modeled by single exponential function (Eq. (3)). The release from sonicated bare MSN, however, was best fit by the double exponential function (Eq. (1)). The parameters for each function are given in Table 2. The double exponential release seen from sonicated MSN is attributed to two different diffusion processes which are discussed in more detail below (see Fig. 8) [19]. We propose that the sonication process enables R6G to penetrate completely into the core of the MSN (Fig. 5) which results in a biphasic release pattern. Conversely, we believe that unsonicated MSN have R6G bound only to the exterior surface (Fig. 5) and thus show a single diffusion process that fits a single exponential function.

After determining how to maximize the MSN's loading capabilities, we studied the effect of pH on release kinetics. Fig. 6 compares the release of rhodamine 6G from unmodified MSN at pH 5.0 and 7.4. At both pH values, there is an initial burst of release within the first 3 h followed by a slower release period that levels off after about 40 h. This result is similar to release from other reported MSN systems [8–14,19]. The rate and amount of release at pH 5.0 is much greater than at pH 7.4 for uncoated MSN. At pH 5.0, the uncoated particles released 3 µg of rhodamine 6G more per mg of MSN than at pH 7.4 (~10.0 µg of rhodamine 6G/mg of MSN at pH 5.0 versus ~7.0 µg of rhodamine 6G/mg of MSN at pH 7.4). This result is consistent with the findings of Tang et al., where the release rate of famotidine from carboxylic acid modified MSU in-

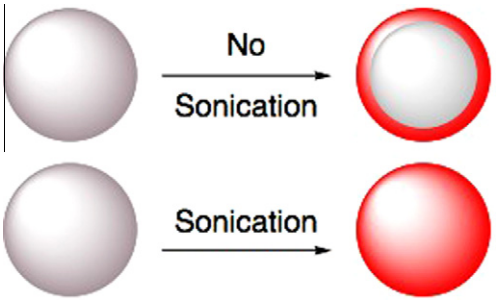

Fig. 5. Schematic representation of the effect of sonication on MSN loading. A: Loading without sonication. B: Loading with sonication.

Table 2
Fit parameters for release of R6G from sonicated and unsonicated MSN at pH7.4.

Sonication	Total release, *P*, (µg/mg) MSN[a]	Percent phase 2, F_2 (%)[a]	k_1, 1/h[a]	k_2, 1/h[a]	Half-life of S_1 (h)[b]	Half-life of S_2 (h)[b]	Phase 1 release, S_1 (µg/mg) MSN[b]	Phase 2 release, S_2 (µg/mg) MSN[b]
Yes	6.78 (12)	48 (15)	1.0 (4)	0.14 (6)	0.69 (17)	4.9 (15)	3.5 (10)	3.3 (10)
No	2.16 (2)	–	1.21 (8)	–	0.58 (3)	–	–	–

[a] In parentheses is the estimated standard error of the fit on the last significant digit(s).
[b] In parentheses is the standard error calculated from the error of the fit on the last significant digit(s).

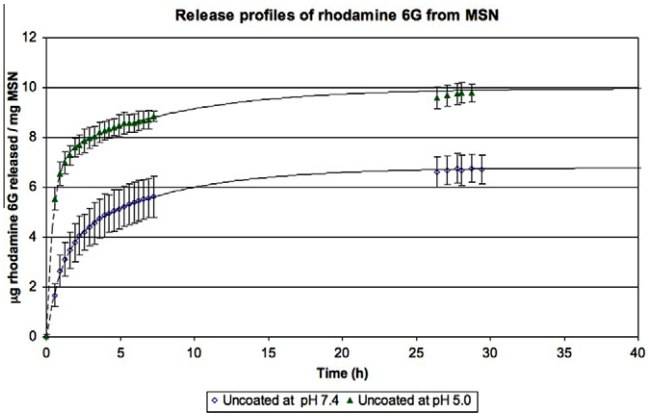

Fig. 6. Release profile of rhodamine 6G from uncoated MSN at pH 7.4 and 5.0.

creased in acidic gastric medium [12]. The increase in rate and amount released can be attributed to decreased electrostatic interactions between the positively charged rhodamine 6G molecules and the silica surface at pH 5.0 (Fig. 7). At pH 7.4, the surface of MSN has a greater negative charge than at pH 5.0, as indicated by the zeta potentials of the particles. At pH 7.4, the particles have a zeta potential of −25.5 mV, while at pH 5.0, the MSN have a zeta potential of −3.40 mV (Table 1).

Both of the release profiles from the bare MSN, at pH 5.0 and 7.4, were better modeled by the two-phase (double) exponential function (Eq. (1)). The fit parameters for release from bare MSN at pH 7.4 and 5.0 are shown in Table 3. From the fit parameters, the half-life and span of each phase were calculated (Table 3).

These results are consistent with the findings of Ng et. al. The authors have shown that the release of rhodamine 6G from bare MSN is biphasic and cannot be described as a simple diffusion process [19]. Using confocal laser scanning microscopy, they have monitored the release of R6G from MSN. Their results show that R6G diffuses from the core of the MSN rapidly and forms a layer of R6G near the exterior of the MSN. The two-phase release profile is attributed to the rapid release from within the interior pores of

Fig. 8. Schematic representation of biphasic release from bare MSN. Phase 1: fast release from center of MSN. Phase 2: slow release from R6G "skin" [19].

the MSN, followed by a more gradual release from the resulting "skin" (Fig. 8). The authors report that the effective rate of diffusion "is almost three times slower in the near edge zone than in the center zone" [19]. And, as time lapses, the diffusion from the center (phase 1 in Fig. 8) becomes less prominent.

Having demonstrated the effect of pH on release from MSN with anionic surfaces, we were interested in seeing how pH affects release from MSN with cationic surfaces. Therefore, we modified the surface of MSN with (3-aminopropyl)triethoxysilane (APTES). Fig. 9 depicts the release profile of rhodamine 6G from APTES-coated MSN at pH 7.4 and 5.0. Though the release profile at pH 7.4 from the amine-coated MSN appears to be similar to the release profile of uncoated MSN at the same pH, there is an initial lag per-

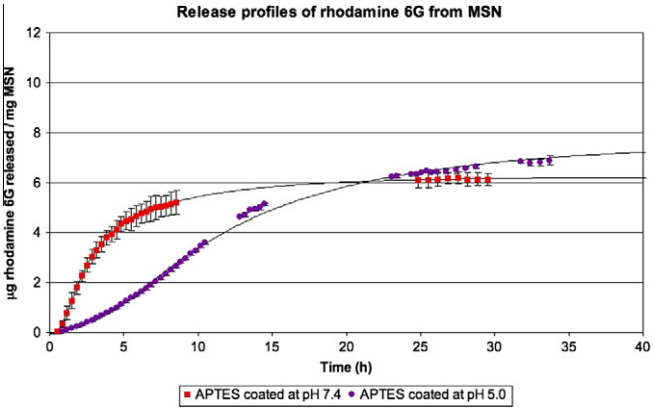

Fig. 9. Release profile of rhodamine 6G from amine-coated MSN at pH 7.4 and 5.0.

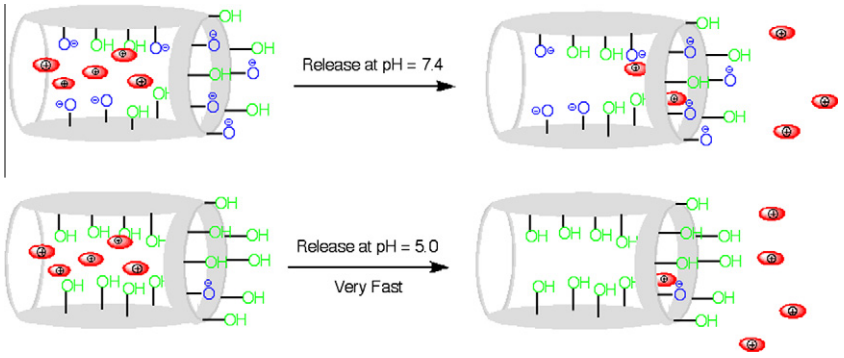

Fig. 7. Schematic representation of release of R6G from MSN at pH 7.4 and 5.0.

Table 3
Two-phase fit parameters for release of R6G from bare MSN.

pH	Total release, P (µg/mg) MSN[a]	Percent phase 2, F_2 (%)[a]	k_1, 1/h[a]	k_2, 1/h[a]	Half-life of S_1 (h)[b]	Half-life of S_2 (h)[b]	Phase 1 release, S_1 (µg/mg) MSN[b]	Phase 2 release, S_2 (µg/mg) MSN[b]
5.0	9.97 (7)	29 (2)	2.3 (2)	0.12 (2)	0.30 (2)	5.6 (6)	7.1 (2)	2.9 (2)
7.4	6.78 (12)	48 (15)	1.0 (4)	0.14 (6)	0.69 (17)	4.9 (15)	3.5 (10)	3.3 (10)

[a] In parentheses is the estimated standard error of the fit on the last significant digit(s).
[b] In parentheses is the standard error calculated from the error of the fit on the last significant digit(s).

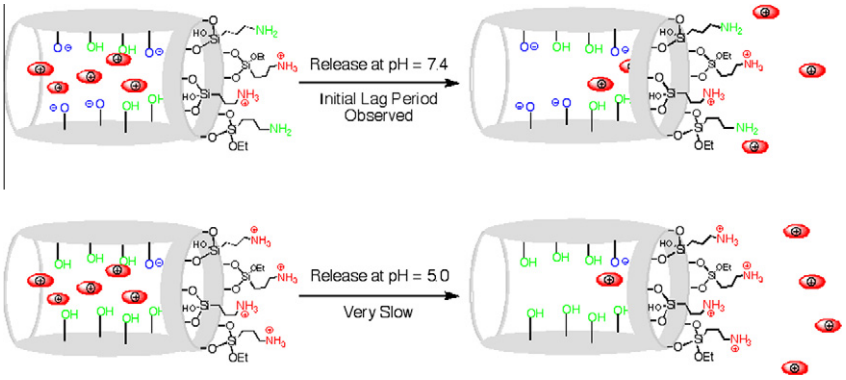

Fig. 10. Schematic representation of release of R6G from APTES-coated MSN at pH 7.4 and 5.0.

iod seen during the first 90 min. Clearly, release from APTES-coated MSN at pH 5.0 is much different than the other release profiles: there is initially a slow release period seen during the first 4 h, which is followed by a faster release phase that begins to level off after about 20 h (Fig. 9). Casasus et al. have reported similar release profiles of a ruthenium dye from polyamine coated MCM-41 at pH 4.0 [13]. However, their analogues 3-aminopropyl functionalized system did not exhibit the same delayed release profile [13]. This difference my be associated with the method used to functionalize the surface of the MSN with APTES. Casasus functionalized MSN with APTES under anhydrous conditions, while we silanized our MSN in PBS solution. It is documented that water promotes multilayer formation during the silanization of silica [45–47]. An APTES multilayer coating would resemble a polyamine coating and would be expected to inhibit the escape of entrapped R6G molecules more so than an APTES monolayer due to the higher charge density that is anticipated. As with the uncoated particles, more total release is seen at pH 5.0 than at 7.4 for the amine coated-MSN. Approximately 7.5 μg of R6G was released per mg of MSN at pH 5.0, while about 6.0 μg of R6G was released per mg of MSN at pH 7.4 (Fig. 9). The initial lag period seen at pH 7.4 and the unique release profile at pH 5.0 seen for the amine-coated MSN can be rationalized by considering the surface coverage and charge of these particles. We hypothesize that the repulsive interaction between the positively charged amine groups and cationic rhodamine 6G molecules inhibit the escape of entrapped R6G molecules within the MSN matrix (Fig. 10). At pH 5.0, the amine groups present on the surface of the MSN are protonated to a greater extent than at pH 7.4, causing the surface of the MSN to be more positively charged at pH 5.0. The zeta potential of APTES-coated MSN is +12.2 mV at pH 7.4 and +41.1 mV at pH 5.0 (Table 1). The increased positive surface charge of the amine-coated MSN can account for the more significant lag period observed at pH 5.0. It should be noted that the basic rhodamine 6G molecules are expected to be protonated and positively charged under both pH conditions. Molecular modeling reported by Casasus et al. suggest that amine monolayers will expand under acidic conditions due to coulombic repulsion between adjacent protonated amine groups [13]. This expanded monolayer will decrease the effective diameter of the pore openings of the MSN and thereby hinder the ability of rhodamine 6G molecules to escape from the MSN matrix. Thus, the decreased dimensions of the pore openings and repulsive interaction between rhodamine 6G and the protonated amine groups located on the surface of the MSN could be the cause of the lag seen at pH 7.4 and the diminished release rate seen at pH 5.0 for these amine-coated MSN.

Interestingly, both of the release profiles from the APTES-functionalized MSN, at pH 5.0 and 7.4, were better modeled by the single-phase exponential (Eq. (3)). The fit parameters and calculated half-life are shown in Table 4.

Table 4
One-phase fit parameters and half-life for release of R6G from APTES-coated MSN.

pH	Total release, P (μg/mg) MSN[a]	k, 1/h[a]	Half-life (h)[b]
5.0	8.46 (15)	0.050 (2)	13.9 (4)
7.4	6.19 (5)	0.23 (1)	3.06 (6)

[a] In parentheses is the estimated standard error of the fit on the last significant digit(s).
[b] In parentheses is the standard error estimated from the error of the fit on the last significant digit(s).

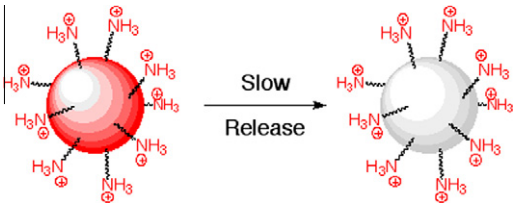

Fig. 11. Schematic representation of single-phase release of R6G from APTES-coated MSN. An R6G "skin" is not formed due to coulombic repulsion.

The two-phase release kinetic of bare MSN and the one-phase release kinetic of APTES-coated MSN can be explained by considering the electrostatic interactions between the surfaces of the bare MSN and amine-coated MSN, respectively, and the cationic R6G. This explanation is drawn from the work of Ng et al. [19]. As stated above, their results show that R6G diffuses from the core of the MSN rapidly and forms a "skin" of R6G toward the exterior of the MSN. The two-phase release profile seen with the bare MSN is attributed to the rapid release from within the interior pores of the MSN, followed by a more gradual release from the resulting "skin" (Fig. 8) [19]. We reason that the amine-coated MSN form very little, if any, "skin" of R6G due to coulombic repulsion. The lack of such a layer of R6G explains why release from APTES-coated MSN is better expressed as a single diffusion process (Fig. 11).

4. Conclusion

The loading and release of rhodamine 6G from unmodified and amine-coated MSN has been studied and the features of this release have been measured. It was found that sonication of MSN in dye solution was necessary to maximize the loading capacity of the particles. It was also determined that both surface modification and pH affect the rate and amount of release from MSN, which

is governed by coulombic interactions. Release from bare MSN at both pH 7.4 and 5.0 followed the same general pattern—an initial burst of release followed by a slower, delayed release period. The increased release from the uncoated MSN at pH 5.0 is attributed to decreased electrostatic interactions between the silica surface and entrapped rhodamine 6G molecules. The initial lag period seen for the amine-coated MSN at pH 7.4 and the unique release pattern seen for the same particles at pH 5.0 can be explained by repulsive interactions between protonated amine groups on the exterior surface of the MSN and rhodamine 6G molecules. Release profiles from APTES-coated MSN better fit a single exponential function while release profiles from bare MSN better fit a double exponential function—indicating that the release of R6G from bare MSN is a two-phase process. Future research will address the effects that pore size, coating thickness, and stronger coulombic interactions have on release dynamics.

Acknowledgements

P. Demuth and M.R. Zachariah acknowledge the generous financial support of the National Science Foundation (NIRT, CHE 0511219478, ''Stimuli-Response Hybrid Nanoparticles for Controlled Chemical Delivery''), the Maryland Technology Development Corporation, and SD Nanosciences, Inc. We gratefully acknowledge shared experimental facilities support from the NSF MRSEC under grant DMR 05-20471. MTH acknowledges the support of the Graduate Assistance in Areas of National Need (GAANN) Fellowship. Partial support for this research was provided to S. Galanie by a grant to the University of Maryland from the Howard Hughes Medical Institute Undergraduate Science Education program and by the Maryland Center for Undergraduate Research Senior Summer Scholars program. We also thank Xiaoxiao He and Dr. Fourkas for their assistance in obtaining BET measurements.

References

[1] C.T. Kresge, M.E. Leonowicz, W.J. Roth, J.C. Vartuli, J.S. Beck, Nature 359 (1992) 710–712.
[2] D. Zhao, J. Feng, Q. Huo, N. Melosh, G. Fredrickson, B. Chmelka, G. Stucky, Science 279 (1998) 548–552.
[3] S.A. Bagshaw, E. Prouzet, T.J. Pinnavaia, Science 269 (1995) 1242–1244.
[4] S. Inagaki, Y. Fukushima, K. Kuroda, J. Chem. Soc. Chem. Commun. (1993) 680–682.
[5] R. Ryoo, J.M. Kim, C.H. Ko, C.H. Shin, J. Phys. Chem. 100 (1996) 17718–17721.
[6] S. Giri, B. Trewn, V. Lin, Nanomedicine 2 (2007) 99–111.
[7] B. Trewn, I. Slowing, S. Giri, H. Chen, V. Lin, Acc. Chem. Res. 40 (2007) 846–853.
[8] M. Vallet-Regi, A. Ramila, R.P. del Real, Perez-Pariente, J. Chem. Mater. 13 (2001) 308–311.
[9] B. Munoz, A. Ramila, J. Perez-Pariente, I. Diaz, M. Vallet-Regi, Chem. Mater. 15 (2003) 500–503.
[10] S.-W. Song, K. Hidajat, S. Kawi, Langmuir 21 (2005) 9568–9575.
[11] W. Xu, Q. Gao, Y. Xu, D. Wu, Y. Sun, W. Shen, F. Deng, J. Solid State Chem. 181 (2008) 2837–2844.
[12] Q. Tang, Y. Xu, D. Wu, Y. Sun, J. Solid State Chem. 179 (2006) 1513–1520.
[13] R. Casasus, E. Climent, M.D. Marcos, R. Martinez-Manez, F. Sancenon, J. Soto, P. Amoros, J. Cano, E. Ruiz, J. Am. Chem. Soc. 130 (2008) 1903–1917.
[14] P. Horcajada, A. Ramila, J. Perez-Pariente, M. Vallet-Regi, Micropor. Mesopor. Mater. 68 (2004) 105–109.
[15] J. Andersson, J. Rosenholm, S. Areva, M. Linden, Chem. Mater. 16 (2004) 4160–4167.
[16] F. Qu, G. Zhu, S. Huang, L. Shougui, J. Sun, D. Zhang, S. Qiu, Micropor. Mesopor. Mater. 92 (2006) 1–9.
[17] M. Stromme, U. Brohede, R. Atluri, A.E. Garcia-Bennet, Nanomed. Nanobiotechnol. 1 (2009) 140–148.
[18] J. Salonen, L. Laitinen, A.M. Kaukonen, J. Tuura, M. Björkqvist, T. Heikkilä, K. Vähä-Heikkilä, J. Hirvonen, V.-P. Lehto, J. Control. Release 108 (2005) 362–374.
[19] J.B.S. Ng, P. Kamali-Zare, H. Brismar, L. Bergstrom, Langmuir 24 (2008) 11096–11102.
[20] C.-Y. Lai, B.G. Trewn, D.M. Jeftinija, K. Jeftinija, S. Xu, S. Jeftinija, V.S.-Y. Lin, J. Am. Chem. Soc. 125 (2003) 4451–4459.
[21] I.I. Slowing, J.L. Vivero-Escoto, C.-W. Wu, V.S.-Y. Lin, Adv. Drug Deliv. Rev. 60 (2008) 1278–1288.
[22] J.L. Vivero-Escoto, I.I. Slowing, C.-W. Wu, V.S.-Y. Lin, J. Am. Chem. Soc. 131 (2009) 3462–3463.
[23] Y. Zhao, B.G. Trewyn, I.I. Slowing, V.S.-Y. Lin, J. Am. Chem. Soc. 131 (2009) 8398–8400.
[24] J. Lu, M. Liong, J. Zink, F. Tamanoi, Small 3 (2007) 1341–1346.
[25] Y.-Z. You, K. Kalebaila, S. Brock, D. Oupichy, Chem. Mater. 20 (2008) 3354–3359.
[26] N.K. Mal, M. Fujiwara, Y. Tanaka, T. Taguchi, M. Matsukata, Chem. Mater. 15 (2003) 3385–3394.
[27] R. Hernandez, H.-R. Tseng, J.W. Wong, J.F. Stoddart, J.I. Zink, J. Am. Chem. Soc. 126 (2004) 3370–3371.
[28] T. Nguyen, H.-R. Tseng, P. Celestre, A. Flood, Y. Liu, J.F. Stoddart, J. Zink, PNAS 102 (2005) 10029–10034.
[29] T. Nguyen, Y. Liu, S. Saha, K. Leung, J.F. Stoddart, J. Zink, J. Am. Chem. Soc. 129 (2007) 626–634.
[30] S. Angelos, Y.-W. Yang, K. Petal, J.F. Stoddart, J.I. Zink, Angew. Chem. Int. Ed. 47 (2008) 2222–2226.
[31] N.M. Khashab, A. Trabolsi, Y.A. Lau, M.W. Ambrogio, D.C. Friedman, H.A. Khatib, J.I. Zink, J.F. Stoddart, Eur. J. Org. Chem. (2009) 1669–1673.
[32] L. Du, S. Liao, H.A. Khatib, J.F. Stoddart, J.I. Zink, J. Am. Chem. Soc. 131 (2009) 15136–15142.
[33] S. Angelos, N.M. Khashab, Y.-W. Yang, A. Trabolsi, H.A. Khatib, J.F. Stoddart, J.I. Zink, J. Am. Chem. Soc. 131 (2009) 12912–12914.
[34] D.P. Ferris, Y.-L. Zhao, N.M. Khashab, H.A. Khatib, J.F. Stoddart, J.I. Zink, J. Am. Chem. Soc. 131 (2009) 1686–1688.
[35] C. Park, K. Oh, S.C. Lee, C. Kim, Angew. Chem. Int. Ed. 46 (2007) 1455–1457.
[36] C.-Y. Hong, X. Li, C.-Y. Pan, J. Mater. Chem. 19 (2009) 5155–5160.
[37] C.-L. Zhu, X.-Y. Song, W.-H. Zhou, H.H. Yang, Y.-H. Wen, X.-R. Wang, J. Mater. Chem. 19 (2009) 7765–7770.
[38] J.C. Beck, J.C. Vartuli, W.J. Roth, M.E. Leonowicz, C.T. Kresge, K.D. Schmitt, C.T.-W. Chu, D.H. Olsen, E.W. Sheppard, S.B. McCullen, J.B. Higgins, J.L. Schlenker, J. Am. Chem. Soc. 114 (1992) 10834–10843.
[39] Y. Lu, H. Fan, A. Stump, T.L. Ward, T. Rieker, C.J. Brinker, Nature (London) 398 (1999) 223–226.
[40] C.J. Brinker, Y. Lu, A. Sellinger, H. Fan, Adv. Mater. (Weinheim, Ger.) 11 (1999) 579–585.
[41] A. Prakash, A.V. McCormick, M.R. Zachariah, Chem. Mater. 16 (2004) 1466–1471.
[42] Y.-S. Lin, C.-P. Tsai, H.-Y. Huang, C.-T. Kuo, Y. Hung, D.-M. Huang, Y.-C. Chen, C.-Y. Mou, Chem. Mater. 17 (2005) 4570–4573.
[43] B. Apostolovic, H.-A. Klok, Biomacromolecules 9 (2008) 3173–3180.
[44] J.C. Groen, L.A.A. Peffer, J. Perez-Ramirez, Microporous Mesoporous Mater. 60 (2003) 1–17.
[45] J.A. Howarter, J.P. Youngblood, Langmuir 22 (2006) 11142–11147.
[46] W. Yoshida, R.P. Castro, J.-D. Jou, Y. Cohen, Langmuir 17 (2001) 5882–5888.
[47] K.M.R. Kallury, P.M. Macdonald, M. Thompson, Langmuir 10 (1994) 492–499.